Towards breaching a still water surface with a miniature unmanned aerial underwater vehicle

Jiaming Zha[1], Eric Thacher[2], Joseph Kroeger[1], Simo A. Mäkiharju[2] and Mark W. Mueller[1]

***Abstract*— Unmanned aerial-underwater vehicles (UAUVs) provide the potential for working on missions in complex multi-domain environments. To achieve amphibian mobility, current UAUV designs rely on additional mechanical components such as multiple layers of propeller blades, water ballast, buoys or wings. This paper presents a miniature UAUV which has a simple mechanical design that resembles a traditional quadcopter. The paper discusses the dynamic modelling, state estimation and control strategy for this UAUV, as well as a detailed characterization of the quadcopter blades operating in the air and water regimes. A strategy for the UAUV to breach calm water surface is then proposed and experimentally tested. The results demonstrate that the UAUV can successfully breach the still water surface, but also show tracking error and breaching delay that are not fully characterized by the model. This suggests the need to carry out further analysis on the dynamics of the UAUV both underwater and in the transition regime.**

I. INTRODUCTION

Unmanned Aerial Vehicles (UAVs) and Autonomous Underwater Vehicles (AUVs) have been used for missions like search and rescue [1] and construction inspection at places that are dangerous to human beings, such as tall bridges [2] and hydroelectric dams [3]. In recent years, there have been attempts to bridge UAVs and AUVs to create hybrid Unmanned Aerial-Underwater Vehicles (UAUVs) that have both aerial and underwater mobility. These vehicles have potentials to work in complicated missions, such as inspecting half-submerged structures like offshore oil platforms and monitoring coastal environment.

To achieve such amphibian capability, a UAUV faces many challenges. First, a UAUV needs to be waterproof, while it has to stay light-weight for efficient flight. Second, a UAUV needs to generate enough thrust in both water and air, two media whose densities differ by three orders of magnitude. Finally, and the focus of this work, a UAUV has to overcome the difficulty of transitioning between water and air.

During the water/air transition, propeller interaction with the fluid interface results in significant variability in the phase fraction of the operating media. This is primarily caused by propeller-induced air entrainment, which is driven by a combination of shear forces at the gas/liquid interface, vortex-induced entrainment, and air entrapment from falling liquid [4]. The interaction of these mechanisms generates a highly unsteady flow field in which the UAUV must operate, making it a difficult challenge for the UAUV to transition between water and air.

The authors are with the [1]HiPeRLab and the [2]FLOW Lab, Department of Mechanical Engineering, University of California, Berkeley, CA 94720, USA. {jiaming_zha,ethacher,jrkroeger,makiharju,mwm}@berkeley.edu

Fig. 1. The Mini Unmanned Aerial Underwater Vehicle. The vehicle has mass of 202g, and a largest linear measure of 14 cm. Shown are three reflective markers used by a motion capture system for in-flight state estimation.

This has led to the development of novel UAUV designs featuring different supportive mechanical structures. For instance, several examples of UAUVs with multiple layers of propellers are seen in literature. Maia et al. presented the Naviator UAUV [5], [6], which features a double-layered propeller design and a hybrid control system. The Naviator makes sure that it can reliably generate thrust during water/air transition, because there are always one set of four propellers clearly underwater, or clearly in the air. Similarly, the Hybrid UAUV, presented in [7], also has two layers of propellers. In additional to four aerial propellers, it has four aquatic propellers with a different leaf number and design to increase underwater mobility. The team also proposed a robust switched control strategy for the Hybrid UAUV system and proved the effectiveness of the controller with high fidelity simulation [8]. Another double-layered design is given in [9], and the researchers use an adaptive sliding mode dynamical surface control approach to transition the UAUV between different media.

An alternate approach for media transition is to use buoyant devices. For example, the Loon copter [10] is a UAUV with a controllable water ballast that can adjust the overall density of the vehicle. To exit the water, the Loon copter will empty its ballast, float to water surface, and then take off when all propellers are cleanly in the air. Similarly,

the Seahawk Alpha drone [11] is designed with a separable buoy. The buoy floats on water surface and is connected to the drone body with cables. Before taking off from water, the drone will reattach itself to the buoy and use the additional buoyancy forces to raise the propellers out of the water.

Lastly, wings are also proposed to help UAUVs with flight. A design that combines underwater gliders and quadcopters is presented in [12]. The resulting vehicle is capable of both vertical take off and horizontal underwater glide.

In this paper, we address the UAUV water/air transition challenge without the help of additional mechanical supports such as dual-layered motor/rotor pairs, variable water ballast, or gliding wings. We present a mechanically simple miniature UAUV system (called the "mini UAUV", and shown in Fig. 1) that resembles normal quadcopters, as well as a transition strategy that helps the mini UAUV to breach still water surface.

The trade-off with a simpler mechanical design is a deeper understanding of the operation of individual components in the air, water, and transition regimes. In particular, since we use a single-layered, instead of a multi-layered setting for propellers, it is necessary to accurately define the performance of the propeller blades in both air and water. Moreover, we constructed a depth estimator to help determine the vertical position of the mini UAUV relative to the free surface. The information enables the mini UAUV to carry out a well-timed transition from underwater to air operation. With the foundation built by the propeller performance analysis and the depth estimator, we manage to achieve a mechanically-simple and low cost vehicle system that has amphibian mobility and can carry out media-transition. The specific focus of this paper is on the mini UAUV's ability to breach the surface under calm water conditions.

The rest of the paper is organized as follows: Section II presents the dynamic modelling of the mini UAUV. Section III introduces the fluid experiments we carried out to characterize the performance of vehicle's propelling system in fluids and during transitions. Section IV outlines the state estimation and control strategy, whereas Section V discusses the hardware design of the mini UAUV and experimental results are presented in Section VI.

II. Modeling of system dynamics

In this section we present the derivation of the translational and rotational dynamics of the system. We will use non-bold letters like m for scalar, bold lower-case letters, such as $\boldsymbol{g}$ for vectors and bold upper-case letters, like $\boldsymbol{J}$ for matrices.

A. Translational dynamics

Fig. 2 shows a simplified representation of the mini UAUV under salient forces. $\boldsymbol{x}_B, \boldsymbol{y}_B, \boldsymbol{z}_B$ are orthonormal bases attached to the body. The mass and mass moment of inertia of the mini UAUV are m and $\boldsymbol{J}$, respectively. Each propeller produces thrust force $f_{P,i}$ in the direction of $\boldsymbol{z}_B$, and r_i denotes the distance between vehicle's center of mass and the propeller thrust force. The buoyancy of the mini UAUV is given by $\boldsymbol{f}_B$ and $\boldsymbol{f}_D$ denotes the drag force the mini UAUV experiences.

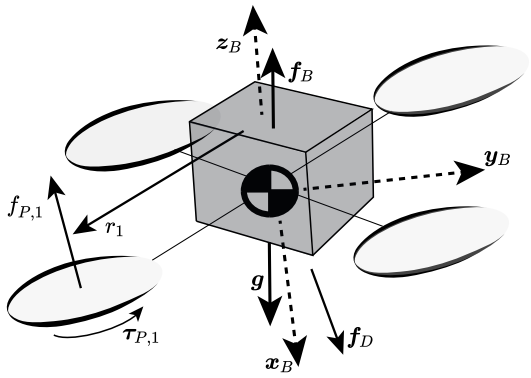

Fig. 2. Model of mini UAUV. Each propeller produces force $f_{P,i}$ and reaction torque $\boldsymbol{\tau}_{P,i}$. The arm-length of the quadcopter is denoted by r_1. The system is also influenced by buoyancy, $\boldsymbol{f}_B$ and drag, $\boldsymbol{f}_D$.

We represent the position of the quadcopter relative to a fixed point in the Earth frame as $\boldsymbol{d} = (x, y, z)$, and the angular velocity as $\boldsymbol{\omega}^B = (p, q, r)$, where p, q, r are the angular velocity in the body frame about $\boldsymbol{x}_B, \boldsymbol{y}_B, \boldsymbol{z}_B$ respectively.

With Newton's second law, we can derive the translational dynamics of the system as:

$$m\ddot{\boldsymbol{d}} = m\boldsymbol{g} + \boldsymbol{R}\boldsymbol{z}\sum_{i=1}^{4} f_{P,i} + \boldsymbol{f}_B + \boldsymbol{f}_D \tag{1}$$

where $\boldsymbol{g}$ represents the gravity vector, $\ddot{\boldsymbol{d}}$ is the acceleration vector of the mini UAUV, $\boldsymbol{z}$ is a unit vector pointing in the direction of $\boldsymbol{z_B}$ and $\boldsymbol{R}$ is a rotational matrix from vehicle body frame to the Earth frame.

According to Archimedes' principle, the direction of buoyancy is opposite to gravity and its value is equal to the weight of the media displaced by the vehicle:

$$\boldsymbol{f}_B = -\rho V \boldsymbol{g} \tag{2}$$

where V denotes the volume of the media displaced and ρ denotes the density of the media.

Meanwhile, drag force is exerted by the fluid in a direction that is opposite to the relative motion of the body with respect to fluid and can be approximated as [13]:

$$\boldsymbol{f}_D = -\frac{1}{2}\rho C_D(Re) A \left\| \dot{\boldsymbol{d}}^F \right\| \dot{\boldsymbol{d}}^F \tag{3}$$

where C_D represents drag coefficients and is a function of shape and Reynolds number. A is the characteristic area of the mini UAUV. $\dot{\boldsymbol{d}}^{\boldsymbol{F}}$ denotes the velocity vector of the vehicle with respect to surrounding fluid. Notice that when the surrounding fluid is stationary with respect to the Earth frame, $\dot{\boldsymbol{d}}^F = \dot{\boldsymbol{d}}$.

We are neglecting the effect of added mass and surface tension which for a small body size are likely to be small in comparison to buoyancy, thrust, and drag.

B. Rotational dynamics

Similar to translational dynamics, we can model the rotational dynamics of the mini UAUV with Euler's Law. Here we use $S(\boldsymbol{a})$ to represent the skew-symmetric matrix form of the cross product, so that $S(\boldsymbol{a})\boldsymbol{b} = \boldsymbol{a} \times \boldsymbol{b}$. Thus, the equation of dynamics can be represented as:

$$\boldsymbol{J}\dot{\boldsymbol{\omega}}^B + S(\boldsymbol{\omega}^B)\boldsymbol{J}\omega^B = \sum_{i=1}^{4}(S(\boldsymbol{r}_i)\boldsymbol{z}_B f_{Pi} + \boldsymbol{z}_B \tau_{Pi}) \quad (4)$$

and the rotational matrix is related to angular velocity through:

$$\dot{\boldsymbol{R}} = \boldsymbol{R}S(\boldsymbol{\omega}^B) \quad (5)$$

Here we are neglecting the moment caused by drag as it is small comparing to the moment generated by propeller thrusts.

III. Vehicle performance in different fluids and during transition

In this section we present the experimentally determined mapping between the input pulse-width modulation (PWM) command signal, motor's rotational speed, and thrust in both air and water for the mini UAUV's electronic speed controller (ESC) and brush-less motor pair, which is 4-in1 DYS 18A BLHeli_S ESC with EMAX 7500KV brushless motor.

The mapping curves are defined in the steady-state region far from the free surface. It was not possible to do so in the air/water transition region as due to the unsteady phase fraction of the fluid interacting with the propeller, steady-state relationships between the command signal, speed, and thrust could not be determined. Rather, we simply characterized the bounds of the transition region, outside of which the free surface has minimal effect on propeller performance.

To simplify fluid-blade interactions, the experiments were conducted using a single propeller blade. The blade was mounted to a RC Benchmark Series 1580 test stand, which measures the thrust from the propeller blade. Rotational speed was measured independently by sampling the change in voltage from a single phase wire; for a three phase, 12-pole motor the rotational speed, ω, is given in units of rad/s by $\omega = (2\pi)6f$ where f is the frequency of voltage fluctuations in the phase wire in Hz. The RC Benchmark test stand was mounted to a Bell-Everman LowBoy linear stage, for which the position was determined with a Renishaw RGH22 encoder with $0.5\mu m$ accuracy. The linear stage was positioned vertically, such that the propeller blades were parallel to the free surface. This setup allowed for precise control of the vertical position of the propeller blade relative to the free surface.

To determine the depth at which free surface effects are important, the propeller was moved smoothly from -55mm to 10mm, for which the rotational speed during successive tests is given in Fig. 3. Three tests were used for command signal values above 1030 PWM, while due to the consistency of the signal only two tests were used for command signal = 1030 PWM.

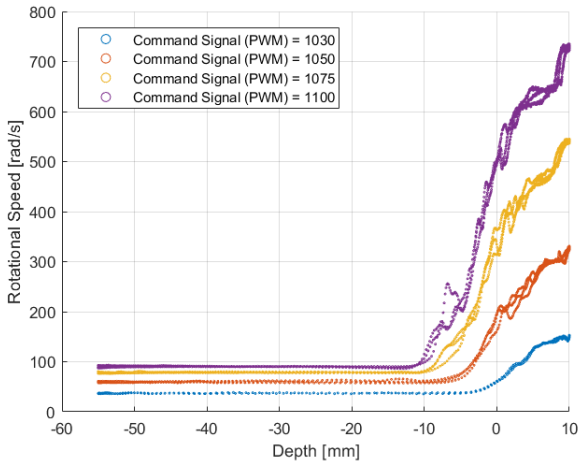

Fig. 3. Propeller speed as a function of depth below free surface.

While lower command signal values reduce the depth at which surface aeration occurs, below -20mm rotational speed converges to a steady state value. Above -20mm, air is entrained below the surface of the water; due to the reduction of density of the surrounding fluid the propeller speed increases. However, the phase fraction of the fluid interacting with the propeller blades is highly variable, which in turn increases the variability of the speed across multiple tests.

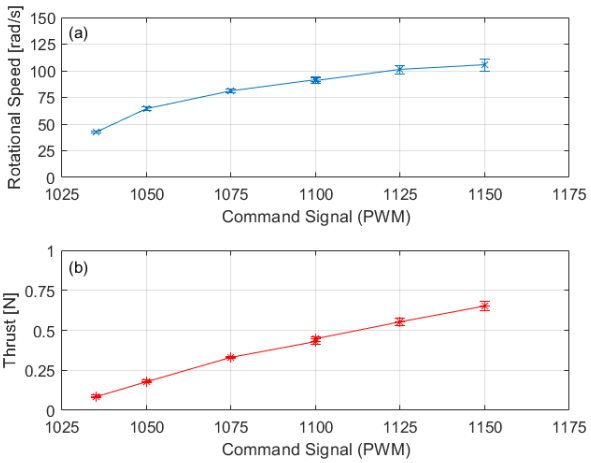

Fig. 4. (a) Rotational speed and (b) thrust as a function of PWM input for operation of propeller blade underwater.

The steady-state thrust and rotational speed of the propeller blade underwater as a function of command signal is given in Fig. 4. The given results are for a depth of -45mm. The buoyancy of the setup below the water is subtracted from the data, such that the thrust is solely generated from the propeller. It's worth noting that the lowest command signal we use for the test is at 1030 PWM, because this is the

lowest PWM signal that can command the brushless motor to spin reliably underwater.

The rotational speed and thrust of the propeller as a function of command signal in air is given in Fig. 5.

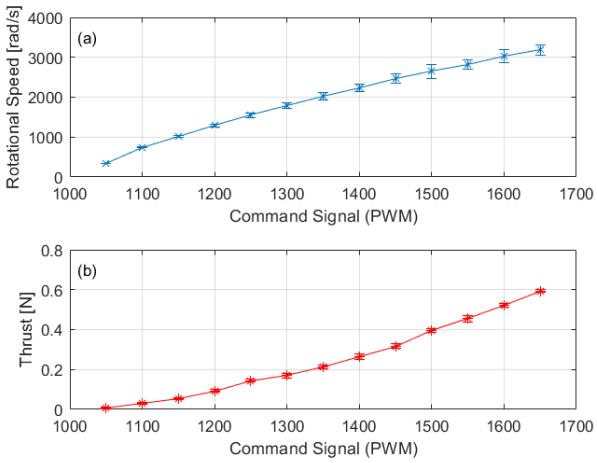

Fig. 5. (a) Rotational speed and (b) thrust as a function of PWM input for operation of propeller blade in air.

Comparing Fig. 4 and Fig. 5, we observe that the relationship between command signal and thrust, defined as command-thrust mapping, depends on the medium the propeller operates in. For example, a 1100 PWM command signal input will generate 0.42N in water, but only 0.03N in air. Clearly, if the command signal were to be kept constant during the transition from water to air, the UAUV would not produce enough thrust to support its own weight. Moreover, with the change of the command-thrust mapping, we also observe a significant shift of the operating range of command signals. Consequently, it is of great importance to accurately identify the medium the mini UAUV operates in and precisely trigger the switch of the control regime at the interface. The control strategy for doing so is described in the following section.

IV. State Estimation and Control Strategy

In this section, we discuss the mini UAUV's sensing system, its depth estimator and its control strategy. It's worth noting that the underwater state estimator is quite different from the one the mini UAUV uses in air, which relies on a motion capture system that can track objects in 3D space. When the mini UAUV operates underwater, it only has access to its IMU and pressure sensor. Thus, it can only estimate its roll, pitch, depth and vertical velocity with confidence.

As a result, the mini UAUV is unable to achieve full 6 DOF autonomy when it operates underwater. Rather, a depth estimator is used to help control the mini UAUV's depth and vertical speed, prior to media-transition.

A. Onboard sensors

The mini UAUV's on-board sensing system is based on an Inertial Measurement Unit (IMU) with 6 degrees of freedom (DOF). In addition, the mini UAUV also features a high precision pressure sensor that provides ambient pressure readings. When in the air, an infrared-based motion-capture system measures position and orientation of the mini UAUV. However, the motion-capture measurement does not work well when the mini UAUV operates underwater because water attenuates the infrared signal reflected by motion-capture markers.

B. Underwater state estimation

When the vehicle operates underwater, we aim to simply estimate its depth, vertical speed, orientation, and angular velocity, while neglecting the horizontal position and velocities. We present a simple Kalman filter for estimating the vertical position and velocity underwater, using measurements from a barometer and the accelerometer.

The vehicle's orientation is estimated using a simple predictor-corrector, relying on the assumption that we directly measure the angular velocity with a rate gyroscope, and measure the acceleration due to gravity using the accelerometer (i.e. the vehicle's linear acceleration is small underwater). This allows us to estimate two components of vehicle's orientation, excluding the yaw component (i.e. the component with respect to $\boldsymbol{z_B}$ axis).

The linear kinematics in the vertical direction of the Earth frame is captured as follows:

$$\begin{bmatrix} \dot{d}_z \\ \dot{v}_z \end{bmatrix} = \begin{bmatrix} 0 & 1 \\ 0 & 0 \end{bmatrix} \begin{bmatrix} d_z \\ v_z \end{bmatrix} + \begin{bmatrix} 0 \\ 1 \end{bmatrix} a_z \tag{6}$$

where d_z is the vehicle's position along the earth-fixed vertical, while v_z and a_z are the vehicle's velocity and acceleration along the vertical. The acceleration along the vertical is estimated using the onboard accelerometer, and a barometer provides depth measurements.

As a result, we can estimate the depth and the vertical velocity of the vehicle with a Kalman filter, assuming constant acceleration over a sampling time T. The barometer reading is linear in the depth, allowing for a straight-forward implementation of a linear, time-varying Kalman filter.

C. In-flight estimation

In flight, the vehicle is visible to a motion capture system, allowing for off-board estimation of the vehicle's full 6-DOF position and orientation states. The on-board rate gyroscope is also used in flight.

D. Control strategy

The overall control strategy of the mini UAUV is captured by Fig. 6, and follows a cascaded control structure as is often used for multicopters. An outer position controller outputs desired thrust and thrust direction, whereas an inner attitude controller outputs desired torques. Finally, a mixer computes per-propeller thrust commands.

The position controller makes position error act as a second order system with damping ratio ζ_p and natural frequency ω_p, as

$$\ddot{\boldsymbol{d}}_d = 2\zeta_p\omega_p(\dot{\boldsymbol{d}}_d - \dot{\boldsymbol{d}}) + \omega_p^2(\boldsymbol{d}_d - \boldsymbol{d}) \tag{7}$$

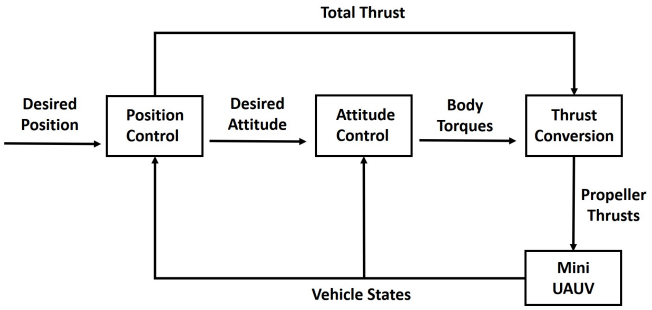

Fig. 6. Controller Architecture of the Mini UAUV

wherein $\ddot{\boldsymbol{d}}_d$ is desired acceleration, $\dot{\boldsymbol{d}}_d$ is desired velocity and $\boldsymbol{d}_d$ is desired position. All vectors are represented in the Earth frame. Thus, we can find desired thrust and its direction as:

$$f_d = m||\ddot{\boldsymbol{d}}_d||_2, \qquad \boldsymbol{z}_{B,d} = \frac{\ddot{\boldsymbol{d}}_d}{||\ddot{\boldsymbol{d}}_d||_2} \tag{8}$$

A desired angular velocity $\boldsymbol{\omega}_d^B$ is computed as proportional to the orientation error as follows: $\dot{\boldsymbol{\omega}}_d^B$ as

$$\dot{\boldsymbol{\omega}}_d^B = \frac{1}{\tau}(\boldsymbol{\omega}_d^B - \boldsymbol{\omega}^B) \tag{9}$$

where $\boldsymbol{\omega}_d^B$ is the desired angular velocity and τ is the desired time constant. All vectors are expressed with respect to vehicle's body frame. Thus, the desired torque follows as

$$\boldsymbol{\tau}_d = J\dot{\boldsymbol{\omega}}_d^B \tag{10}$$

With desired body-torque and desired total thrust, we can compute the desired thrust force for each propeller with a quadcopter mixer presented as follows:

$$f_{P_i} = \frac{1}{4}\left(\begin{bmatrix} r_{i,y}^{-1} & -r_{i,x}^{-1} & \kappa^{-1} \end{bmatrix} \boldsymbol{\tau}_d + f_d \right) \tag{11}$$

where $r_{i,x}$ and $r_{i,y}$ are the components of $\boldsymbol{r}_i$ in the $\boldsymbol{x}_B$ and $\boldsymbol{y}_B$ directions and κ is the propeller torque constant.

The same controller is used underwater and in the air, with the notable difference that the desired underwater horizontal acceleration is always identically zero.

E. Transition strategy between underwater and air operation

As is discussed in Section III, the command-thrust mapping and command signal operating range in water is significantly different from that in air. If an erroneous mapping is used, the mini UAUV would generate thrusts that are far away from desired, and fail to breach the water. As a result, the key to a successful water/air transition is to switch the command-thrust mapping from underwater mode to air mode at the interface. Moreover, it is desirable to carry out the mapping switch when the propellers are exposed to air rather than fully submerged in water, as using the air command-thrust mapping underwater will generate an unexpected large thrust that can potentially destabilize the system.

Based on the above, we came up with a three step transition guideline that is illustrated in Fig. 7 and described as follows:

1) Accelerate towards water surface with underwater command-thrust mapping.
2) Breach the water surface. Switch to air command-thrust mapping when all propellers are exposed to air.
3) Proceed flying in air with air command-thrust mapping.

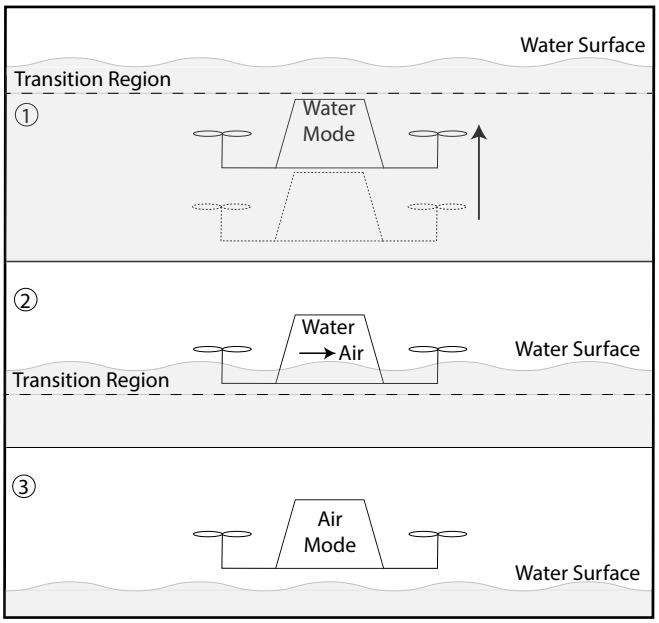

Fig. 7. Illustration of mini UAUV's breaching strategy

While accelerating towards the water surface, the depth estimator is used to track the vertical position and velocity of the mini UAUV. However, once the mini UAUV enters the transition region, the location of which is characterized in Section III, air entrainment alters the medium density and we can no longer reliably calculate depth based on the pressure reading. Hence, the depth estimator cannot tell us the exact time at which the mini UAUV breaches the water.

To solve the problem, we start a timer once the the mini UAUV reaches the transition region. During breaching, the mini UAUV has an strict time window in which the propellers are exposed to air. We can switch the mini UAUV to air command-thrust mapping when the timer reading falls in this time window.

We estimate this time window with the force balance on the body in the vertical direction, which is given in Eq. (1). To simplify the model, we assume the mini UAUV as a prism. It has a base area A, and its volume is uniformly distributed along its height, h. We define $z_{surface}$ as the vertical position of the water surface and z_t as the vertical position of the prism's top surface, both in the Earth frame. Then, when $z_{surface} < z_t < z_{surface} + h$ the buoyancy force can be given as:

$$f_{B,z} = \rho g A(h + z_{surface} - z_t) \tag{12}$$

Meanwhile, the drag force in the vertical direction can be derived from Eq. (3) as:

$$f_{D,z} = -\frac{1}{2}\rho C_D(Re)A|\dot{z}_t|\dot{z}_t \tag{13}$$

Hence, we can estimate the vertical motion of the vehicle with the following ordinary differential equation:

$$\ddot{z}_t = -g + \frac{\rho g A(h + z_{surface} - z_t)}{m} - \frac{\rho C_D(Re)A|\dot{z}_t|\dot{z}_t}{2m} \tag{14}$$

Notice that effect of the thrusts is ignored here, because when the vehicle operates in the air with the underwater command-thrust mapping, the thrusts generated are small in comparison to buoyancy and drag.

We can solve Eq. (14) numerically using the position and velocity at the start of the breaching event to obtain the estimated time window. Due to the uncertainty associated with the density of the surrounding fluid and resulting forces, this is computed offline and used as a benchmark value after which the switching time is manually tuned.

V. Hardware design of mini UAUV

To build a miniature UAUV capable of breaching the water surface, we need to fulfill the following design requirements:

First, the vehicle is small-scale, lightweight, yet still negatively buoyant (i.e. the gravity force acting on it is larger than the buoyancy force), so that the vehicle can both sink underwater and operate in the air. Second, the whole vehicle system should be water-proof. Third, the on-board pressure sensor should have access to the pressure information of surrounding media so as to provide readings for the depth estimator.

In order to meet these requirements, we created a system featuring the following designs:

A. Vehicle frame and aviation stack

To minimize the size, we build a small vehicle frame and a highly compact aviation stack.

As can be seen in Fig. 1, the vehicle features a lightweight carbon fiber frame with an arm length of 65mm manufactured by water-jet and four EMAX 7500KV high thrust-to-weight ratio brushless motor.

The onboard aviation stack is composed of a Bitcraze Crazyflie 2.0 [14] chip as an integrated computation and sensing unit, and a 4-in1 DYS 18A BLHeli_S ESC to drive the brushless motors. Additional auxiliary circuits, including power regulators and voltage dividers are arranged on a custom-made printed circuit board. All electronic components are powered by a single 2-cell 800mAh LiPo battery. Laser-cut mounting adapters were designed to help assemble the electronic stack vertically and minimize the space it takes.

B. Waterproof housing with membrane

To waterproof the mini UAUV, we fabricate a housing shell encasing all on-board electronics via 3D-SLA-printing. An O-ring groove that docks a 55mm ID O-ring is engraved at bottom of the shell to provide sealing between the shell and carbon fiber frame. To pass ambient pressure information to the on board pressure sensor, we build the top of the shell with a 1mm-thick latex membrane. As the latex membrane is highly flexible, it equalizes the air pressure in the shell to ambient water pressure. As a result, we are able to directly measure surrounding water pressure from inside the shell.

VI. Experimental validation

To assess the ability of the mini UAUV to operate in water, air, as well as the transition regime, an experiment was conducted of the mini UAUV breaching the water surface in calm water. In doing so, the mini UAUV demonstrates the ability to transition between underwater and air operation autonomously.

A. Physical parameters

The physical parameters of the mini UAUV are listed in table 1.

TABLE I
MINI UAUV PHYSICAL PARAMETERS

Parameter	Value
m	$0.202\,\mathrm{kg}$
V	$186 \times 10^{-6}\,\mathrm{m}^3$
I_{xx}	$112 \times 10^{-6}\,\mathrm{kg\,m}^2$
I_{zz}	$187 \times 10^{-6}\,\mathrm{kg\,m}^2$
$f_{P_i,max}$	$1.1\,\mathrm{N}$
$\|\|\boldsymbol{r}_i\|\|_2$	$0.065\,\mathrm{m}$
$\|\kappa_i\|$	$808 \times 10^{-5}\,\mathrm{m}$

B. Experiment setup and the test trajectory

The experiment is designed to verify the water breaching strategy proposed in Section IV. Ideally, the mini UAUV should accelerate towards the free surface, breach the surface and then keep flying in air to a desired height.

We carry out the breaching strategy by commanding the mini UAUV to follow a two phase trajectory. Initially, the vehicle is placed 0.15m below water surface, on the bottom of a water tank. When the program starts, the off board controller first commands the mini UAUV to track a trajectory with an initial desired vertical velocity of $1\mathrm{m/s}$ and a desired vertical acceleration of $2\mathrm{m/s}^2$. This phase lasts for 1.3s and the trajectory is used to ensure that the mini UAUV smoothly rises through the water to the free surface. After 1.3s, the controller will check if the mini UAUV is successfully detected by the motion capture system. If yes, the trajectory enters phase two and the off board controller commands a desired vertical position of 1m above water surface, with zero desired velocity and acceleration. Otherwise, an emergency stop of the mini UAUV is triggered.

The test is carried out in a lab space equipped with motion capture system and an off board controller sends radio commands to the mini UAUV at a rate of 50Hz.

When tracking the aforementioned trajectory, the mini UAUV breaches the water with a velocity of about $0.5\mathrm{m/s}$. Using an initial estimate from Eq. (14) and subsequent tuning, we program the controller to switch command-thrust mapping 0.08s after the mini UAUV detects that it reaches

the transition region. Last, it is worth noting that we disable mini UAUV's yaw control and only control its roll and pitch (i.e. its orientation with respect to $\boldsymbol{x_B}$ and $\boldsymbol{y_B}$ axis) during phase 1, because we don't have a reliable yaw measurement underwater. After the vehicle is detected by the motion capture system and enters phase 2, we re-enable the full attitude control.

C. Result and analysis

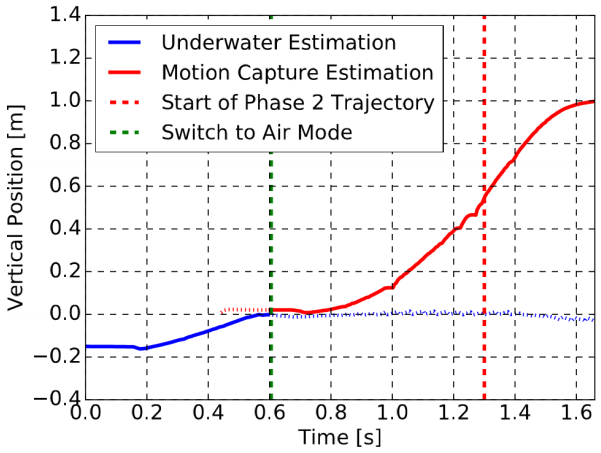

Fig. 8. Estimated vertical position of the mini UAUV during test.

Fig. 8 shows the estimated vertical position of the mini UAUV during the test. We define zero datum at the water surface. The blue curve shows the estimation provided by mini UAUV's underwater depth estimator, whereas the red curve shows the estimation provided by the motion capture system. Due to the nature of these estimates, their accuracy depends on the medium within which the UAUV operates. In particular, when the UAUV is outside of water the pressure-based depth estimator is unable to differentiate changes in position. Furthermore, due to signal attenuation of the motion capture infrared signal, the motion capture system is unable to provide accurate estimates underwater. With this in mind, when position estimates cannot be trusted, the readout is plotted as dotted curve. The red vertical line shows when the vehicle enters phase 2 of the trajectory and the green vertical line denotes when the mini UAUV switches from underwater mode to air mode.

The mini UAUV reaches the transition region at about t = 0.5s. However, instead of continuing to rise, the mini UAUV loses its initial momentum and stays on top of the free surface for about 0.2 seconds. While 0.08s is spent switching control regimes, the cause for the remaining 0.12s delay is not fully understood. Potential causes for this delay are the time needed for propeller spin-up and the generation of turbulence on the water surface from propeller-fluid interaction. Particularly, once the UAUV switches to air mode, the resulting increase in rotational speed induces significant air/water mixing in the fluid surrounding the propeller blades. Since the control strategy produces a command signal based on expected rotational speed and thrust, an unsteady operating medium would prevent the desired thrust from being generated. This phenomena is also captured for a single propeller in Fig. 3, which shows an increased variability in rotational speed during the transition regime.

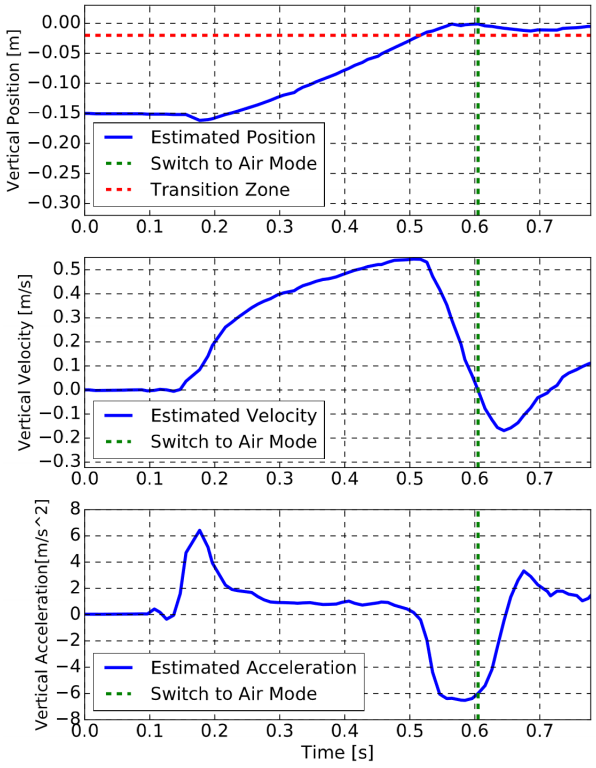

Fig. 9. Estimation of mini UAUV's vertical position, velocity and acceleration underwater and during the transition phase.

In addition to the above challenges, from Fig. 8 we can see that the mini UAUV does not track the acceleration trajectory well underwater. This indicates a discrepancy between our model and reality, which may be caused by underestimation of the drag effects underwater and not considering the added mass effect.

Fig. 9 illustrates in detail the estimation of the mini UAUV's motion underwater and during the water/air transition phase. The estimation of vertical position and velocity is provided by the depth estimator described in Section IV and is based on both barometer and inertial measurement unit readings, whereas the estimation of vertical acceleration is purely based on readings of inertial measurement unit. The horizontal red dotted line marks the beginning of the transition region and the vertical green dotted line denotes where the mini UAUV switches from underwater mode to air mode.

We can see that the switch to air mode occurs when the velocity of the UAUV is about 0m/s. This shows that the spin up of the propellers takes place when the mini UAUV is about to lose all its momentum and starts dropping back to

water. Moreover, from the acceleration plot, we can observe that the acceleration increases after the mini UAUV switches to air mode, suggesting an increase in thrust. At about 0.7s, the velocity turns positive and the mini UAUV starts to climb, marking the end of the breaching phase. The UAUV then follows the command to 1m above water surface.

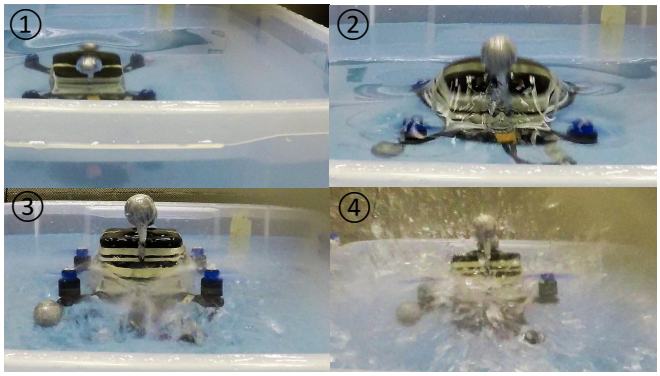

Fig. 10. Image sequence showing the mini UAUV breaching the water surface.

Fig. 10 showcases an image sequence of mini UAUV's water breach. In picture 1, the vehicle accelerates towards water surface with underwater command-thrust mapping. In picture 2, the top of the vehicle breaches water surface. In picture 3, all propellers leave water surface and the vehicle switches to air command-thrust mapping. In picture 4, the vehicle fully leaves water and starts flying in the air.

The experiment demonstrates that the mini UAUV is able to carry out a transition from water to air. Meanwhile, it is noteworthy that we see a discrepancy between the commanded trajectory and the actual trajectory carried out by the mini UAUV, showing that we need to further improve our dynamic model, especially for the parts when the mini UAUV is underwater and during transition phase.

The video of the experiment can be found at `https://hiperlab.berkeley.edu/mini-uauv/`

VII. CONCLUSIONS

This paper presents a mechanically simple miniature UAUV that can autonomously breach a calm water surface without additional mechanical supports. It features an on-board depth estimator that provides information about the vehicle depth and its rate of change. A transition strategy of accelerating towards water surface and then switching command-thrust mapping is proposed and verified with experiment.

For future research, we will further investigate the dynamic model of the mini UAUV when it operates underwater and during the transition phase to minimize the discrepancy between our current model and reality. Moreover, we want to extend the mini UAUV's ability to carry out media transition under various environmental conditions, including rough waves.

REFERENCES

[1] S. Waharte and N. Trigoni, "Supporting search and rescue operations with uavs," in *Emerging Security Technologies (EST), 2010 International Conference on*. IEEE, 2010, pp. 142–147.

[2] N. Metni and T. Hamel, "A uav for bridge inspection: Visual servoing control law with orientation limits," *Automation in construction*, vol. 17, no. 1, pp. 3–10, 2007.

[3] P. Ridao, M. Carreras, D. Ribas, and R. Garcia, "Visual inspection of hydroelectric dams using an autonomous underwater vehicle," *Journal of Field Robotics*, vol. 27, no. 6, pp. 759–778, 2010.

[4] A. Durve and A. Patwardhan, "Numerical and experimental investigation of onset of gas entrainment phenomenon," *Chemical Engineering Science*, vol. 73, pp. 140–150, 2012.

[5] M. M. Maia, D. A. Mercado, and F. J. Diez, "Design and implementation of multirotor aerial-underwater vehicles with experimental results," in *Intelligent Robots and Systems (IROS), 2017 IEEE/RSJ International Conference on*. IEEE, 2017, pp. 961–966.

[6] D. A. M. Ravell, M. M. Maia, and F. J. Diez, "Modeling and control of unmanned aerial/underwater vehicles using hybrid control," *Control Engineering Practice*, vol. 76, pp. 112–122, 2018.

[7] P. L. Drews, A. A. Neto, and M. F. Campos, "Hybrid unmanned aerial underwater vehicle: Modeling and simulation," in *Intelligent Robots and Systems (IROS 2014), 2014 IEEE/RSJ International Conference on*. IEEE, 2014, pp. 4637–4642.

[8] A. A. Neto, L. A. Mozelli, P. L. Drews, and M. F. Campos, "Attitude control for an hybrid unmanned aerial underwater vehicle: A robust switched strategy with global stability," in *Robotics and Automation (ICRA), 2015 IEEE International Conference on*. IEEE, 2015, pp. 395–400.

[9] Z. Ma, J. Feng, and J. Yang, "Research on vertical air–water trans-media control of hybrid unmanned aerial underwater vehicles based on adaptive sliding mode dynamical surface control," *International Journal of Advanced Robotic Systems*, vol. 15, no. 2, p. 1729881418770531, 2018.

[10] H. Alzu'bi, I. Mansour, and O. Rawashdeh, "Loon copter: Implementation of a hybrid unmanned aquatic–aerial quadcopter with active buoyancy control," *Journal of Field Robotics*, 2018.

[11] "Seahawk alfa prototype completes dock chain inspection," Feb 2019. [Online]. Available: https://flyswimfly.com/news/2019/2/12/seahawk-alfa-prototype-completes-dock-chain-inspection

[12] D. Lu, C. Xiong, B. Lyu, Z. Zeng, and L. Lian, "Multi-mode hybrid aerial underwater vehicle with extended endurance," in *2018 OCEANS-MTS/IEEE Kobe Techno-Oceans (OTO)*. IEEE, 2018, pp. 1–7.

[13] B. R. Munson, T. H. Okiishi, A. P. Rothmayer, and W. W. Huebsch, *Fundamentals of fluid mechanics*. John Wiley & Sons, 2014.

[14] W. Giernacki, M. Skwierczyński, W. Witwicki, P. Wroński, and P. Kozierski, "Crazyflie 2.0 quadrotor as a platform for research and education in robotics and control engineering," in *Methods and Models in Automation and Robotics (MMAR), 2017 22nd International Conference on*. IEEE, 2017, pp. 37–42.